NASA

Technical Memorandum 86059

ON THE REMOTE SENSING OF CLOUD PROPERTIES FROM SATELLITE INFRARED SOUNDER DATA

HWA-YOUNG M. YEH

FEBRUARY 1984

National Aeronautics and
Space Administration

Goddard Space Flight Center
Greenbelt, Maryland 20771

ON THE REMOTE SENSING OF CLOUD PROPERTIES FROM SATELLITE INFRARED SOUNDER DATA

Hwa-Young Yeh

NAS/NRC Research Associate

Severe Storms Branch

Goddard Laboratory for Atmospheric Sciences

NASA/Goddard Space Flight Center

Greenbelt, MD 20771

February 1984

Contents

PRECEDING PAGE BLANK NOT FILMED

PAGE ii INTENTIONALLY BLANK

Figures

Tables

ABSTRACT

A method for remote sensing of cloud parameters by using infrared sounder data has been developed on the basis of the parameterized infrared transfer equation applicable to cloudy atmospheres. The method is utilized for the retrieval of the cloud height, amount, and emissivity in 11 μm region. Numerical analyses and retrieval experiments have been carried out by utilizing the synthetic sounder data for the theoretical study. The sensitivity of the numerical procedures to the measurement and instrument errors are also examined. The retrieved results are physically discussed and numerically compared with the model atmospheres. Comparisions reveal that the recovered cloud parameters agree reasonably well with the pre-assumed values. However, for cases when relatively thin clouds and/or small cloud fractional cover within a field of view are present, the recovered cloud parameters show considerable fluctuations.

Experiments on the proposed algorithm are carried out utilizing High Resolution Infrared Sounder (HIRS/2) data of NOAA 6 and TIROS-N. Results of experiments show reasonably good comparisons with the surface reports and GOES satellite images.

1. Introduction

Satellite measurements can provide global coverage of cloud properties such as cloud top height and temperature, fractional cloud cover and cloud emissivity. Those data are essential for the inclusion of cloud parameterizations in realistic models of the earth's climate (Schneider, 1972; Cess, 1974; Stephens and Webster, 1979). Recently, the World Climate Research Programme (WCRP) plan recognized the need to develop a uniform global cloud climatology as part of a broad research program on climate processes. The International Satellite Cloud Climatology Project (ISCCP) thus has been approved as the first project of WCRP. The basic objective of the ISCCP is to collect and analyze satellite radiance data to infer the global distribution of cloud radiative properties in order to improve the modeling of cloud effects on climates.

The purpose of this research is to explore the algorithm retrieving the cloud properties by utilizing the available infrared sounder data from polar-orbiting satellites. Although the geostationary meteorological satellite measurements are used as the primary operational data for the ISCCP, the polar-orbiting satellites are essential to the project providing 1) coverage of the high latitude regions not viewed by the geostationary satellites; 2) a basis for normalization of the radiances observed by the different geostationary satellites; 3) global coverage that may help mitigate the possible loss of one or more geostationary satellites; 4) multispectral measurements for discriminating cloud properties not derivable from the primary two-channel geostationary data (Schiffer and Rossow, 1983). In addition to the HIRS data on polar-orbiting satellites, the VISSR Atmosperic Sounder (VAS) data of GOES satellites (Smith et al., 1981) can also be applied to the current proposed algorithm in future.

In this study, two channels of 15 µm CO_2 assorption band and one channel of 11 µm window region are used for the retrieval of cloud top height, fractional cloud cover and emissivity of 11 µm region. The application of sounder data to cloud parameters retrieval has been investigated previously. McCleese and Wilson (1976), Smith and Platt (1978) and Wielicki and Coakley (1981) have demonstrated that cloud heights and effective cloud cover can be recovered under a wide variety of atmospheric conditions using different regions in the near and far infrared parts of the terrestrial spectrum. Also, recently, Chahine (1982) applied 15 µm infrared radiance data for day and night mapping of the global distributions of the horizontal cloud covers and the corresponding cloud top pressure levels. His results showed that the effective cloud cover derived from 15 µm data is less than that obtained from visible data. The discrepancy is obviously due to the existence of nonblack clouds in the atmosphere. It is therefore important for us to determine the cloud emissivity and "physical cloud cover" separately in the retrieval. Only such cloud cover can be compared with values obtained from nephanalysis of visible cloud images.

In the following sections, we present the basic formulation of the upwelling radiance in cloudy atmospheres and the technique for the cloud parameters retrieval. Numerical experiments and a number of case studies utilizing the HIRS/2 data for the retrievals are then described and physically discussed.

2. Cloud Parameters Retrieval

Consider an atmosphere containing fractional cloud cover A within a satellite instantaneous field-of-view (IFOV). The emitted radiation intercepted by the satellite radiometer can be written in the equation calculating the upwelling radiance at top of the atmosphere,

$$\tilde{I}(\nu_i,\theta,\infty) = AI^c(\nu_i,\theta,\infty)+(1-A)I(\nu_i,\theta,\infty), \tag{1}$$

where $I(\nu_i,\theta,\infty)$ is the clear-column mean spectral upwelling radiance measured in a channel whose mean effective wavelength is ν_i and the local zenith angle of the observation is θ. If we consider only the thermal emission in the atmosphere at longwave infrared frequencies, $I(\nu_i,\theta,\infty)$ can be described by the solution of the radiative transfer equation under the condition of thermodynamic equilibrium,

$$I(\nu_i,\theta,\infty) = B(\nu_i,T_S)T(\nu_i,\theta;\infty,0)+\int_0^\infty B[\nu_i,T(Z)]K(\nu_i,\theta;\infty,Z)dZ, \tag{2}$$

where B is the spectral Planck function associated with temperature T, T is the spectral transmittance for the relevant gas, T_S is surface temperature, and $K(\nu_i,\theta;\infty,Z)=dT(\nu_i,\theta;\infty,Z)/dz$ is the spectral weighting function. In Eq. (1), $I^c(\nu_i,\theta,\infty)$ is the upwelling radiance emitted from cloudy area, and can be derived in terms of the cloud and atmospheric radiative properties. This radiance is caused by 1) the transmission of the upwelling radiance from the cloud layer, 2) the emission from the cloud top, and 3) the emission and absorption contribution of the gases above the cloud top. Their mathematical expressions can be written in the following forms,

$$\begin{aligned} I(\nu_i,\theta,\infty) = {} & \{I(\nu_i,\theta,Z_t)T^c(\nu_i,\theta) \\ & +B[\nu_i,T(Z)][1-T^c(\nu_i,\theta)]\}T(\nu_i,\theta;\infty,Z_t) \\ & +\int_{z_t}^{\infty} B[\nu_i,T(Z)K(\nu_i,\theta;\infty,Z)dZ, \end{aligned} \tag{3}$$

where Z_t is cloud top height, and $T^c(\nu_i,\theta)$ the cloud transmissivity which is function of the cloud thickness and optical properties. The upwelling radiance from the atmosphere below the cloud layer $I(\nu_i,\theta,Z_t)$ can be expressed in terms of the radiative transfer equation

$$\begin{aligned} I(\nu_i,\theta,Z_t) = {} & B(\nu_i,T_S)T(\nu_i,\theta;Z_t,0) \\ & +\int_{0}^{z_t} B[\nu_i,T(Z)]K(\nu_i,\theta;Z,Z)dZ. \end{aligned} \tag{4}$$

In writing the preceding equations, the surface infrared emissivity is assumed to be unity, and the cloud reflectivity is considered to be negligible (e.g., Paltridge and Platt, 1976). The cloud radiative properties are described by the cloud transmissivities which depend on the temperature structure and the total water path in the vertical column of the cloud. All quantities given in the above equations are integrated over wavenumber, and weighted by the spectral response of the instrument. However, since B varies slowly with ν, while T varies rapidly and without correlation to B within the narrow spectral channels of the HIRS/2, it suffices to perform the spectral integrations of B and T independently and treat the results as if they were monochromatic values for the effective wavenumber (Yeh and Liou, 1983; Smith, 1983). We thus may change the reference layer of clear column transmittances and weighting functions from cloud layer to the top of the atmophere in Eq. (4),

$$T(\nu_i,\theta;\infty,Z) = T(\nu_i,\theta;Z_t,Z)T(\nu_i,\theta;\infty,Z_t) \tag{5}$$

$$K(\nu_i,\theta;\infty,Z) = K(\nu_i,\theta;Z_t,Z)K(\nu_i,\theta;\infty,Z).$$

For simplicity, we eliminate θ in the equations, replace ν_i by i to indicate the channel number, and define $T(\nu_i,\theta;\infty,z)=T_i(z)$ and $K(\nu_i,\theta;\infty,z)=K_i(z)$. On substituting Eqs. (2), (3), (4) and (5) into (1), we obtain parameterized equation for the upwelling radiance emergent from a partially, single-layer cloudy atmosphere in the form

$$\tilde{I}_i(\infty) = I_i(\infty)-A(1-T_i^c)I_i'(Z_t), \tag{6}$$

where

$$I_i'(Z_t) = B_i(T_S)T_i(0)+\int_0^{Z_t} B_i[T(Z)]K_i(z)dZ-B_i(Z_t)T_i(Z_t). \tag{7}$$

In Eq. (6), two terms on the right-hand side represent, respectively, the clear-column radiance and the correction of the first term due to the cloud contamination within the IFOV. For multiple-layer cloudy atmospheres, Eq. (6) will be used as if the lower clouds are attached to the top-layer cloud, and their combination can be viewed as one thick cloud. In the absence of the cloud, $A=0$ and $T_i^c=1$, the Eq. (6) reduces to $\tilde{I}_i(\infty)=I_i(\infty)$.

a. Cloud top height determination

Let the difference between the upwelling radiances for clear and cloudy atmospheres be

$$\Delta G_i = I_i(\infty)-\tilde{I}_i. \tag{8}$$

To a good approximation, the cloud transmissivities may be considered to be the same for the adjacent channels within HIRS/2 15 μm interval. That is, where i and j are two adjacent channels in the 15 μm CO band. We define the ratio to the radiance differences for i and j channels as

$$H(Z_t) = \frac{\Delta G_i}{\Delta G_j} = \frac{I_i'(Z_t)}{I_i'(Z_t)} \tag{9}$$

Because of the ratio, the H function is independent of the cloud opacity, and depends only on the weighting function of the channels and the radiance profile from the surface to the cloud top. Since the weighting function varies slightly with changing temperature and water vapor profiles, the approximate relation between the H value and Z_t may be constructed through Eq. (9) with a given radiance profile $B_i(Z)$. By evaluating the radiance profile from radiosonde observations or climatological profiles, we may determine Z_t from the value of ΔG_i and ΔG_j, which are obtained from Eq. (8) when observed radiance $\tilde{I}_i$ and the clear column radiance $I_i(\infty)$ are used. $I_i(\infty)$ may be computed based on the available radiosonde profiles. It should be noted that degree of the polynomial relating Z_t and H value may affect the accuracy of the results. More detailed discussion will be given in the section on numerical experiments.

The method of using adjacent channels within 15 μm region for cloud height inference has been discussed previously (e.g., Smith and Platt, 1976; Wielicki and Coakley, 1981; Yeh et al., 1984). No further discussion about the method will be repeated here.

(b) Cloud amount and emissivity determination

The radiance of HIRS/2 channel 7 (at 13.4 μm) and channel 8 (at 11 μm) are mostly contributed from the gaseous emission in the lower atmosphere and the surface for the clear atmosphere in view of the distribution of weighting functions (Fig. 1). Both channels are sensitive to the presence of clouds at any altitude. For nonblack clouds, the cloud radiative properties at these two frequencies are distinct, but the relationship of their radiative properties can be used in determining the cloud parameters.

Assume that the cloud transmissivity may be approximately expressed as an exponential function of the cloud optical depth τ which is the product of the volume absorption coefficient β_i and the geometric thickness

$$\begin{aligned} T_i^c(\Delta Z) &= \exp(-\tau_i) \\ &= \exp(-\beta_i \Delta Z). \end{aligned} \tag{10}$$

One classical problem of computing the radiative transfer within clouds is defining the medium in the sense that no operational model is likely to predict the drop size distribution as a function of height within the cloud. The predictable parameters will probably be restricted to either liquid and/or ice water content per volume w or the total water content W in the vertical column of the cloud. The grossest approximation is simply

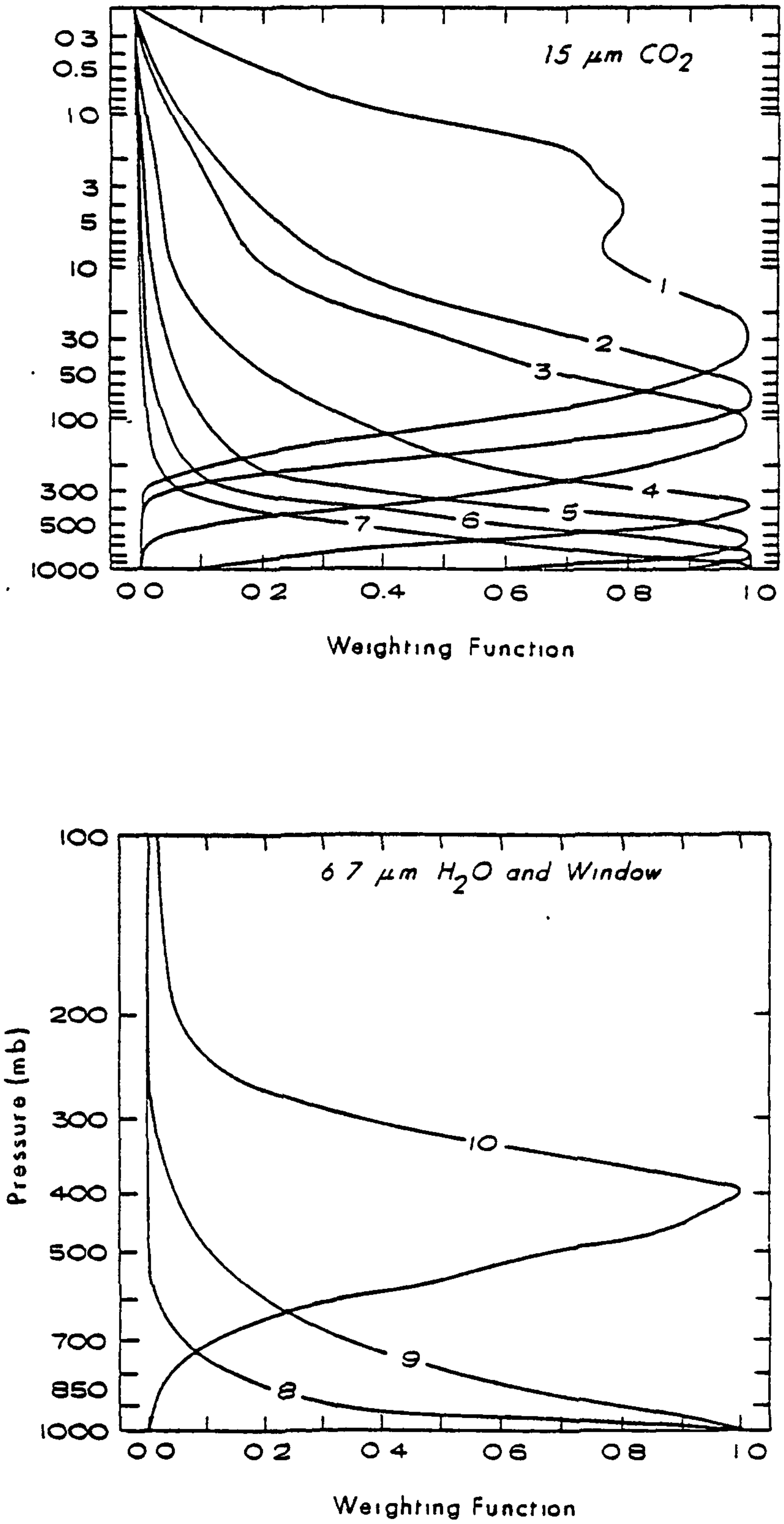

Fig 1. HIRS/2 Weighting Functions: Weighting functions of the HIRS/2 15 μm CO_2, 6.7 μm H_2O and window channels.

to assign one volume absorption coefficient to each cloud type, irrespective of the variations in cloud water content and drop size distributions. The volume absorption coefficient then represents a mean radiative property to each cloud type.

If possible it is obviously preferable to relate the volume absorption coefficient as directly as possible to water content w. The ideal case is of a cloud which has a unique drop size distribution, since then β_i is simply proportional to the total number of drops per unit volume and therefore to w. Paltridge and Platt (1976) found that some fairly simple relation does exist between β_i and w. They showed that the value of $d\beta_i/dw$ for 11 μm is nearly a constant, and therefore

$$\beta_i = \kappa_i w \tag{11}$$

The parameter $\kappa_i (= d\beta_i/dw)$ is in fact the mass absorption coefficient by the above definition. Such a relation is valid approximately for the entire window region of the spectrum from 8 to 14 μm.

Considering two narrow spectra centering at 11 and 13.4 μm, the experiments by Feddes and Lious (1978) show that $r = \kappa_{13.4\ \mu m}/\kappa_{11\ \mu m}$ is approximately equal to 1.1 for both ice and water clouds. If we insert Eq. (10) to Eq. (6), and apply the consequence to the two channels of 11 and 13.4 μm, we may obtain the following equation

$$px - qx^r - (p-q) = 0, \tag{12}$$

where

$$p = (\tilde{I}_7 - I_7) I_8'(Z_t)$$

$$q = (\tilde{I}_8 - I_8) I_7'(Z_t) \tag{13}$$

$$x = T_8^c.$$

The subscripts 7 and 8 in the equations denote the channel number of the HIRS/2. It is readily seen that one may apply iterative method solving x in Eq. (12). Solution of x is the cloud transmissivity at 11 μm, and is always within (0,1). The cloud emissivity in 11 μm region can then be obtained by the following approximation

$$\varepsilon = 1 - x. \tag{14}$$

And the fractional cloud cover is

$$A = (\tilde{I}_8 - I_8)/\varepsilon I_8'(Z_t). \tag{15}$$

One should know that solving x in Eq.(12) is not an easy task, because the noises from the measured radiances affecting the coefficients p and q in the equation. The difficulties concerning numerical calculations will be discussed in the next section.

3. Numerical experiments and theoretical analyses

a. Numerical procedures

In this section, we construct a hypothetical cloudy atmosphere and perform numerical calculations of atmospheric parameters in order to test the validity of the foregoing derivations. The error sensitivity of the numerical procedures will also be examined. The measurement errors are introduced into theoretical calculations, and results of the errors generated in the sequential computations are analyzed.

In the error analysis, we use the radiosonde profile of Charleston, S.C., at 1200 (all times GMT), 24 April 1980 as the model atmosphere filled with various types of clouds in an IFOV. The "measured" radiances are simulated for a range of 10 cloud amounts (0.1 to 1.0), 3 cloud top heights (300 mb to 700 mb) and 6 cloud optical thickness in 11 μm region (0.5 to 3.0). In calculating the measured radiances, we introduce a Gaussian random noise distribution to the temperature and water vapor profiles. These random noises, which are to be added to 40 values of temperature and water vapor concentration, are determined by an inverse Gaussian probability distribution function. The standard deviations used for the temperature and water vapor profiles are $1^{o}k$ and 20%, respectively.

After this is done, we then impose some artificial errors on to the "measured" values to simulate instrumental noises. The noise is taken to be Gaussian with zero mean and a standard deviation of 0.22 $mWm^{-2}sr^{-1}cm$ for the 15 μm channels according to the noise levels specified for the HIRS/2 instrument on TIROS-N (Schwalb, 1978). For each cloud amount, optical depth, and cloud top height combination, 200 samples are then constructed in order to investigate the statistical properties of the retrieved quantities.

Before we display the results of the calculations, we shall discuss the difficulties of solving Eq. (12) first. Although the solution of x has to be within the domain of (0,1), there is a solution x=1 (clear atmosphere) always satisfies Eq. (12). While the given measurement errors, which affect the values p and q, cause the failure of finding a solution within (0,1), x=1 will be automatically obtained as the solution. However, this solution may not be acceptable for many cases. Especially when the cloud optical depth is large, and true solution is close to the left margin of the domain (0,1), one may easily fail to find a solution within (0,1). To minimize such mistakes, some criteria must be imposed to reexamine the solution if x is found to be 1.

To illustrate the statements given above, the cloud-free (x=1) percentages for the various cloud amount and optical depth combinations are plotted and shown in Fig. 2. Without imposing any criteria, the cloud-free percentage obtained by solving Eq. (12) is as expected decreasing with increasing optical depth from 0.5 to 1.5. This is due to the fact that the larger cloud signatures are sensed from thicker clouds by the satellite radiometer than those from thinner clouds. Therefore, less probability of cloud-free atmosphere is obtained for thicker cloud. However, the cloud-free percentage rises when the optical depth is greater than 1.5. This is because the cloud transmissivity becomes smaller (more opaque) for the thicker clouds, and the same amount of measurement error may cause higher opportunity of failing to find a solution within (0,1). Since x=1

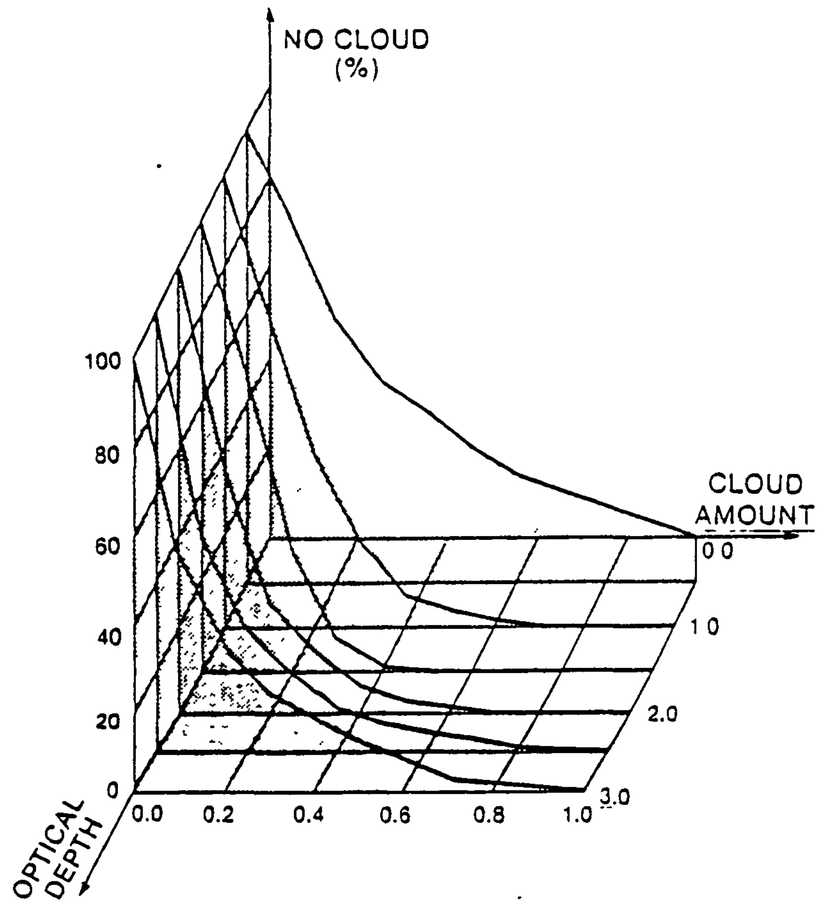

Fig. 2 Cloud Amount versus Optical Depth (no criteria imposed): Cloud-free percentage for cloud height at 300 mb based on the calculation without imposing criterion (see text for details) for various cloud amount and optical depth combinations

automatically becomes the solution for such a no-solution situation, cloud-free percentage thus increases incorrectly.

By examining Eq. (12), we find that for the smaller value of the constant term p-q, the influence from measurement errors on the solution x becomes greater proportionally. Recalling Eq. (13), we may have

$$\Delta pq = p-q = I_7'(Z_t)I_8'(Z_t)[T_8^c(Z_t)-T_7^c(Z_t)]A. \tag{16}$$

It is readily seen that Δpq is linearly dependent on the cloud transmissivities and cloud amount. In Fig. 3, it shows that Δpq generally decreases with increase of cloud optical depth τ if $\tau>1$, but increases with increase of τ if $\tau<1$. When a cloud is optically thick enough (or a black cloud), Δpq should be close to 0, irrespective of the change of cloud amount. For clouds with the given cloud transmissivities, Δpq is 0 when A=0, and is a maximum value when A=1 (overcast). Actually, Δpq can have negative values when the measurement errors are involved in the cases of small cloud amount or optically thick cloud. (For optical very thin clouds, Δpq may also be negative, but the solution of x should be close to 1 anyway; no correction will be attempted in this situation.)

If we evaluate the difference between the measured radiances of 11 and 13.4 μm channels, we find that

$$\begin{aligned}\Delta\tilde{I} = \tilde{I}_8-\tilde{I}_7 &= (I_8-I_7)-A(1-T_8^c)[I_8'(Z_t)-I_7'(Z_t)] \\ &+ pq/I_8'(Z_t).\end{aligned} \tag{17}$$

Results of $\Delta\tilde{I}$ are also plotted on Fig. 3. It shows that $\Delta\tilde{I}$ has the maximum value when no cloud is present within IFOV, but declines with increase of cloud amount. In Eq. (17), when the optical depth increases, the second term on the right-hand side becomes more important, and $\Delta\tilde{I}$ becomes smaller or even a negative value. From Fig. 3, we find that the tendencies of $\Delta\tilde{I}$ and Δpq are oposite with variation in cloud amount. Since the value of $\Delta\tilde{I}$ decreases with increase of cloud amount, the differentiation of clear or cloudy atmospheres by comparing $\Delta\tilde{I}$ with a criterion become feasible. Let us define

$$R_0 = (I_8-I_7)-\Delta pq/I_8'(Z_t), \tag{18}$$

then

$$\Delta\tilde{I} > R_0, \quad \text{clear;} \tag{19}$$

otherwise, cloudy. Note that the dimension of $\Delta pq/I_8'(Z_t)$ is the same as $\Delta\tilde{I}$, and Δpq contains the information of cloud amount and cloud optical depth (or emissivity) as Eq. (16) implies. In the program, Δpq is obtained from the direct result of Eq. (13).

To display the response of values of Δpq and ΔI to the change of radiosonde profile, we also plot Δpq and $\Delta\tilde{I}$ with variations in cloud amount and optical depth for tropical and midlatitude winter climatological profiles (Figs. 4 and 5). The basic patterns remain the same with only difference of the stretches of Δpq and $\Delta\tilde{I}$. These values obtained by using midlatitude winter climatological profile apparently are within narrower

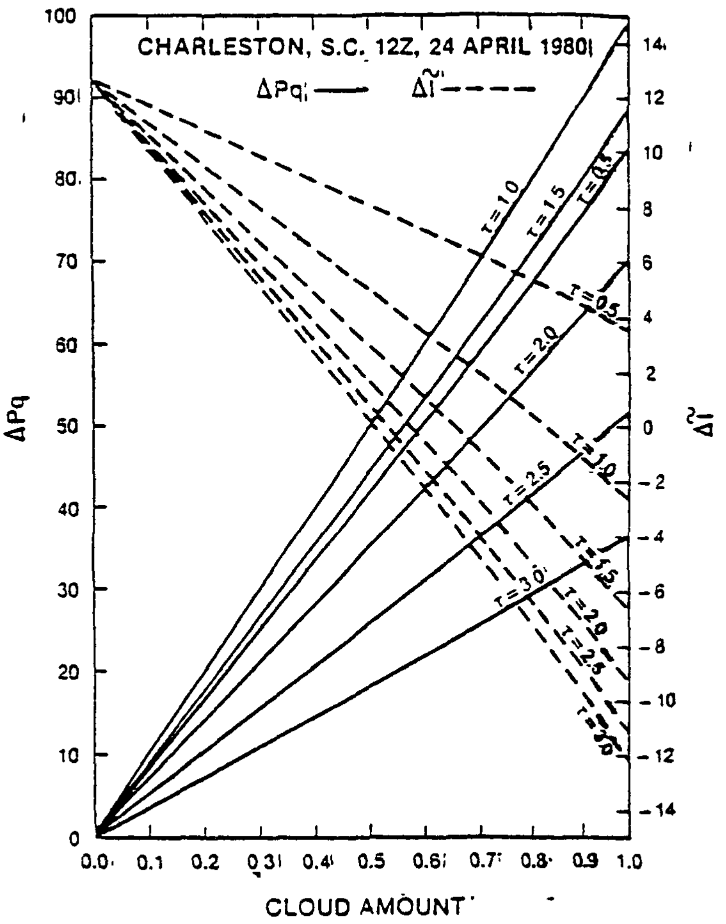

Fig. 3. Cloud Amount versus Δpq and $\Delta\tilde{I}$ (Charleston, SC)

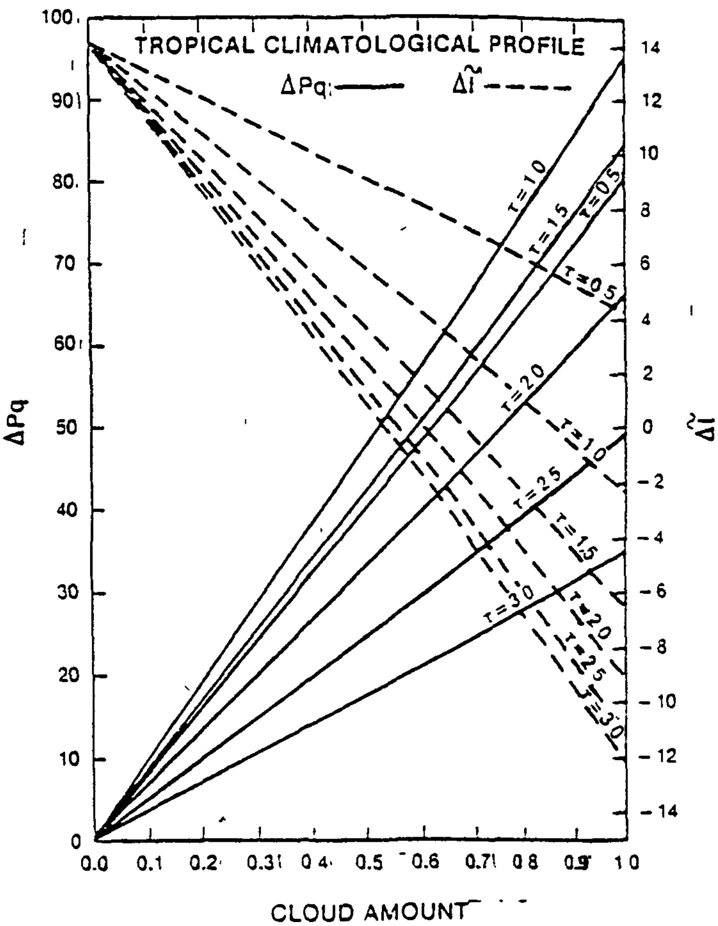

Fig. 4. Cloud Amount versus Δpq and $\Delta\tilde{I}$ (Tropical climate profile).

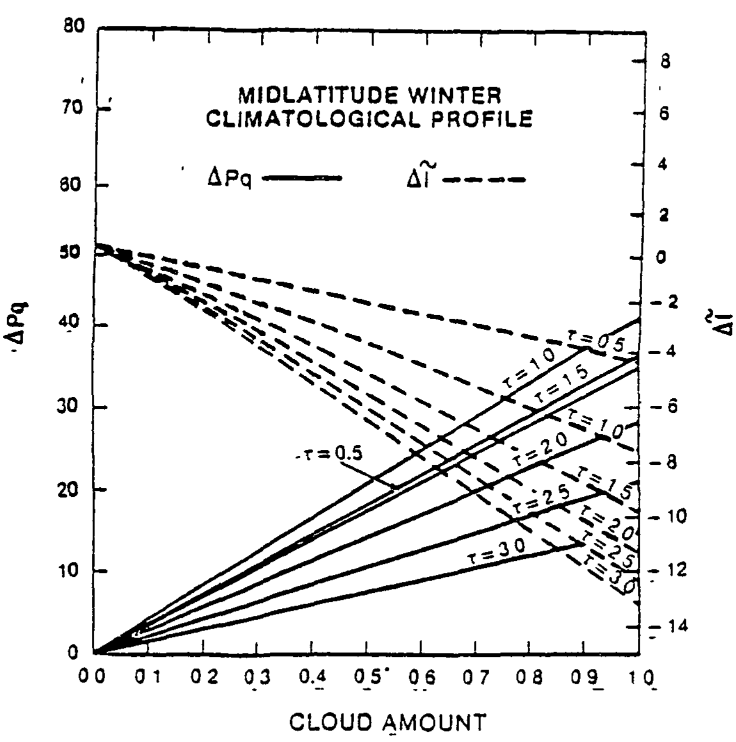

Fig. 5 Cloud Amount versus Δpq and $\Delta\hat{I}$ (Midlatitude winter profile)

region due to colder profile and the less distinctive upwelling radiances profiles from channels 7 and 8. In contrast, the values using the tropical climatological profile show wider stretches of Δpq and $\Delta\tilde{I}$ due to warmer radiosonde profile and more distinctive upwelling radiances in two channels.

After reevaluating the solution of x=1 to determine if it is actually clear or cloudy atmosphere, it is desirable to further retrieve the cloud parameters based on the following procedures. It should be known that the results from the following discrete differentiation method is less sensitive to the measurement errors, although may not be as accurate as the solutions directly solved from Eq. (12). Again, the value of Δpq can be used as a guideline for the criteria. If the values of Δpq become negative, we shall expect the solutions to be large cloud optical depth (or emissivity) and/or small cloud amount. Since emissivity is always within (0,1), we decide to estimate emissivity in stead of optical depth, which, theoretically speaking, is between 0 and infinity.

For the cases of $\Delta pq<0$, let us assume

$$R_m = [(I_8-I_7)+\Delta pq/Z_8'(Z_t)]-S_m[I_8'(Z_t)-I_7'(Z_t)],$$

$$m=1,\dots,5, \tag{20}$$

where $S_1=0.03$, $S_2=0.05$, $S_3=0.09$, $S_4=0.15$ and $S_5=0.23$, then

$$\begin{aligned} \Delta\tilde{I}&>R_1, && \varepsilon=0.20;\\ R_1>\Delta\tilde{I}&>R_2, && \varepsilon=0.40;\\ R_2>\Delta\tilde{I}&>R_3, && \varepsilon=0.60;\\ R_3>\Delta\tilde{I}&>R_4, && \varepsilon=0.80;\\ R_4>\Delta\tilde{I}&>R_5, && \varepsilon=0.95; \end{aligned} \tag{21}$$

Otherwise, $\varepsilon=1.00$.

Should $\Delta pq>0$ occur, we may assume

$$R_n=[(I_8-I_7)-\Delta pq/I_8'(Z_t)]-S_n[I_8'(Z_t)-I_7'(Z_t)],$$

$$n=6,\ldots,10, \tag{22}$$

where $S_6=0.075$, $S_7=0.15$, $S_8=0.20$, $S_9=0.275$ and $S_{10}=0.35$, then

$$\begin{aligned}
\Delta\tilde{I}&>R_6, & A&=0.10;\\
R_6>\Delta\tilde{I}&>R_7, & A&=0.25;\\
R_7>\Delta\tilde{I}&>R_8, & A&=0.40;\\
R_8>\Delta\tilde{I}&>R_9, & A&=0.55;\\
R_9>\Delta\tilde{I}&>R_{10}, & A&=0.70;
\end{aligned} \tag{23}$$

Otherwise, $A=0.90$. After solving either cloud emissivity or cloud amount from the above procedures, we then may go back to Eq. (6) to solve cloud amount or emissivity.

It should be explained the reasons that we find cloud emissivity in Eq. (21) for the solution, while we find the cloud amount in Eq. (23). Let us tabulate the number distribution of positive and negative values of Δpq for the solution $x=1$ derived from 200 samples at each cloud amount and optical depth combination (Table 1). We then further convert the number distribution to the percentage distribution by dividing the numbers of

Table 1. Δpq Distribution: Number and percentage distribution for the positive and negative values of Δpq for cases x=1 in 200 samples at each cloud amount and optical depth combination

A \ τ	0.5 (+)	0.5 (-)	1.0 (+)	1.0 (-)	1.5 (+)	1.5 (-)	2.0 (+)	2.0 (-)	2.5 (+)	2.5 (-)	3.0 (+)	3.0 (-)
0.1	8	52	14	51	19	52	17	68	13	67	12	78
(%)	13	87	22	78	27	73	20	80	16	84	7	93
0.2	19	35	18	36	15	42	16	54	8	66	6	78
(%)	35	65	33	67	26	74	23	77	11	89	7	93
0.3	32	24	25	19	6	22	4	41	0	48	0	61
(%)	57	43	57	43	21	79	9	91	0	100	0	100
0.4	36	13	13	2	4	11	2	27	0	33	0	54
(%)	74	26	87	13	27	73	7	93	0	100	0	100
0.5	34	5	8	4	1	5	0	14	0	24	0	45
(%)	87	13	67	33	17	83	0	100	0	100	0	100
0.6	33	2	4	1	0	2	0	4	0	18	0	28
(%)	94	6	80	20	0	100	0	100	0	100	0	100
0.7	35	0	1	0	0	1	0	3	0	12	0	22
(%)	100	0	100	0	0	100	0	100	0	100	0	100
0.8	37	0	-	-	-	-	-	-	0	12	0	23
(%)	100	0							0	100	0	100
0.9	33	0	-	-	-	-	-	-	0	6	0	23
(%)	100	0							0	100	0	100
1.0	28	0	-	-	-	-	-	-	0	6	0	10
(%)	100	0							0	100	0	100

either positive or negative value of Δpq by their sum and multiplying 100 as percentage. Results of the percentage distribution for the positive and negative values of Δpq are plotted in Fig. 6.

In Fig. 6, the percentage distributions of positive values of Δpq are denoted by the numbers without parenthesis, and those of negative values are marked by the numbers with parentheses. Since the total percentage must be 100%, all the contours are shared by both positive and negative percentages. The areas without coverage of contours are the sections which pose no controversy of obtaining $x=1$ in cloudy atmospheres. It shows in Fig. 6 that the higher percentage of positive values generally distributes in the areas of thinner cloud (or lower emissivity); while the negative values distribute more in the areas of thicker cloud. Furthermore, the gradient of positive value distribution is parallel to the abcissa (cloud amount), but the gradient of negative value distribution is oriented along with the ordinate (cloud optical depth). Therefore, it is desired to find the cloud amount directly if Δpq is positive, and find the cloud emissivity if Δpq is negative.

b. Application of the cloud retrieval program to HIRS/2 channels.

The NOAA 6 satellite was launched on 27 June 1979. It is a third generation operational, sun-synchronous, near polar orbiting satellite with a height of about 810 km and having morning descending or afternoon ascending. Successive orbits cross the equator with 98.74 degrees of inclination and the orbital period is about 101.26 min.

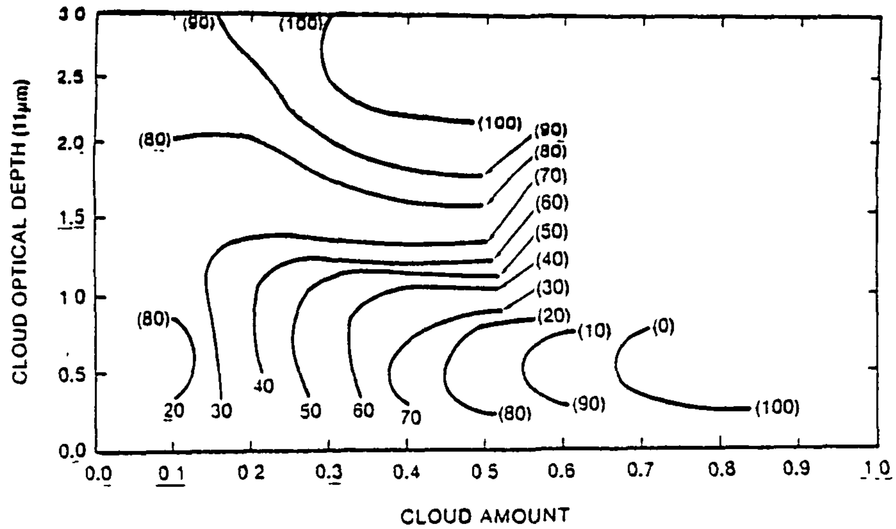

Fig. 6. $\Delta\sigma q$ Distribution Plots. Percentage distribution of positive and negative (with parentheses) values of $\Delta\sigma q$

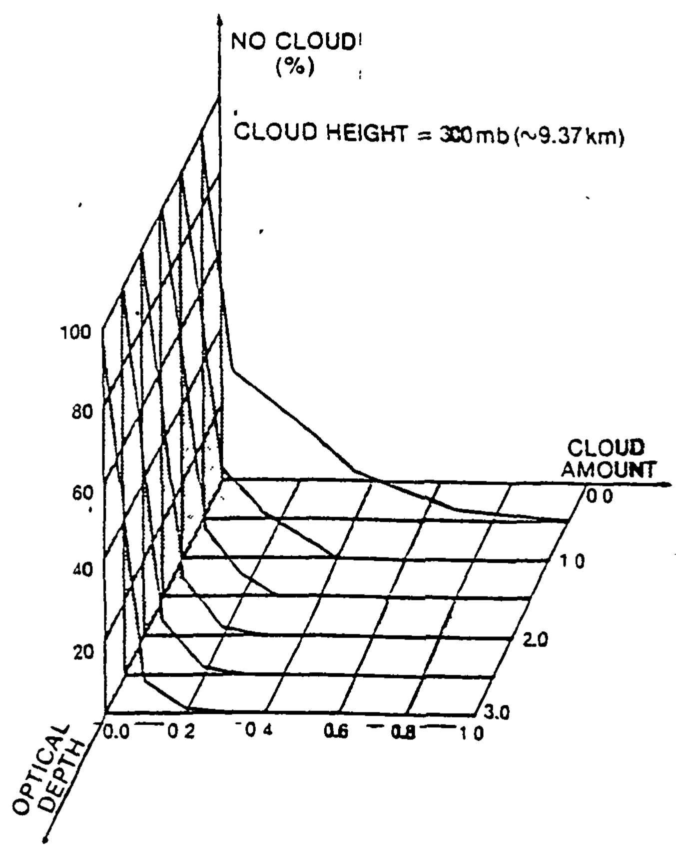

Fig. 7a Cloud Amount versus Optical Depth (restrictive criteria imposed) for Cloud Ht at 300 mb.

The NOAA 6 HIRS/2 instrument is an adaptation of the HIRS/1 instrument designed for and flown on the Nimbus 6 satellite. This instrument, being built by the Aerospace/Optical Division of ITT, measures incident radiation in 20 spectral regions of the infrared spectrum, including both longwave (15 μm) and shortwave (4.3 μm) regions. The instrument cross-track scans ±49.5 (±1120 km) to satellite subtrack. There are 56 scan steps per scan line with a resolution of 17.4 km near nadir and 29.9 km at the extremes of the scan.

The data that are routinely processed at NOAA/NESDIS are available on nine-track, 1600 bpi tapes. The data of each orbit were packed in such a way that 20 channels of data were stored separately in 20 files. These data have been rearranged to contain co-located radiance values for all 20 channels. The data set to be used in this analysis will be 24 April 1980, during which all channels of the HIRS instrument were operating properly.

In numerical computations, the simulated atmosphere will be divided in such a manner that it coincides with the presssure levels used in the clear column radiance program (CCR) developed at NOAA/NESDIS. There are 40 pressure levels for the CCR program. The program utilizes predetermined transmission profiles which can be empirically adjusted as a function of the known temperature and moisture profiles. The transmittance programs were kindly provided by L. McMillin. The weighting functions of the HIRS channels are depicted in Fig. 1. We will use three HIRS channels including two in the 15 μm CO_2 band for cloud height retrieval and combining 15 μm band wing channel and the 11 μm window channel for cloud amount and emissivity calculations. The retrieved cloud parameters will be compared with available surface observations and satellite pictures to assess the reliability of the proposed cloud detection technique utilizing the existing data. In the course of this investigation, a concept of mapping various clouds over the globe may be developed and proposed for future satellite experimentation.

c. Results of numerical calculation.

Results of the sequential calculations for the cloud top height, cloud amount and emissivity are plotted in Figs. 7, 8 and 9. The figures show the mean value (bias) and standard deviation (S.D.) of 200 samples for each cloud amount and optical depth combination. The measurement and instrument errors, which are created randomly as described in the last section, are imposed onto the exact "measured" radiances for the theoretical calculations.

First, we assume the cloud height is at 9.37 km, which is approximately equivalent to 300 mb for the midlatitude spring climatological profile. By giving various combinations of cloud amount and optical depth, we shall examine the bias and stability of the alogrithm. The probability of this alogrithm miscalculating a cloudy atmosphere as a clear atmosphere or vise versa is shown in Fig. 7a. In addition to the criterion as described eariler to differentiate clear and cloudy atmospheres if $x=1$, we set another criterion such that if either ΔG_i or ΔG_j in Eq. (9) is equal to or less than 0 , the atmosphere is assumed to be clear. We found that the probability of mistreating a clear atmosphere as a cloudy atmosphere is generally less than 2%. However, for cloudy atmospheres with cloud amount equal to 0.1, we have about 38% of chance miscalculating them as clear atmospheres for $\tau=0.5$ or 7% for $\tau=3.0$. The cloud-free percentage clearly decreases with increase of cloud optical thickness even if the optical depth is greater than 1.5. This, of course, is the result of the treatments reevaluating the solution x=1 as described in the last section. When the fractional cloud cover increases within IFOV, the cloud-free probability decreases rapidly, especially for optically thick clouds.

For the cases we have determined as cloudy atmospheres, we then calculate the mean cloud height by averaging the solutions of those cloudy cases. Results show that the mean cloud heights are generally overestimated (Fig. 7b). This is particularly evident for optically thin clouds and/or small fractional clouds within IFOV. The S.D. shows that the stability of the cloud height retrieval is less satisfactory for optically thin clouds and the small fractional clouds. The S.D. decreases significantly with the increases of cloud amount and optical depth.

The mean cloud amounts are estimated in such a manner that the results of the computations for the entire 200 samples are used for computing the mean values and S.D. (Fig. 7c). This means that for cloudy atmospheres which are miscalculated as clear atmospheres in the algorithm, results of A=0 will be counted in the estimations of mean cloud amount and the S.D. The outcome is as expected that the mean cloud amounts for optically thin clouds are underestimated. This is because the larger percentage of optically thinner clouds are mistreated as cloud-free in the alogrithm. However, the cloud amounts are generally overestimated if $\tau>1$. The outcome of the S.D. also shows that the algorithm is less stable when a optically thin cloud is present in the atmosphere. The underestimation of the cloud amount is also found for the case which is assumed to be nearly overcast.

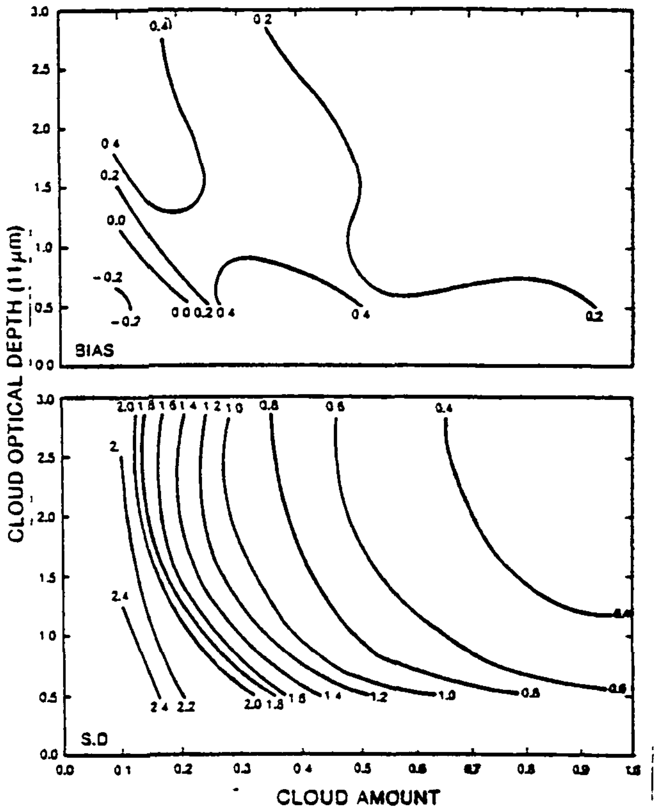

Fig. 7b Bias and Standard Deviation of Computed Cloud Height for Various Assumed Amounts and Optical Depths (cloud heights assumed at 300 mb)

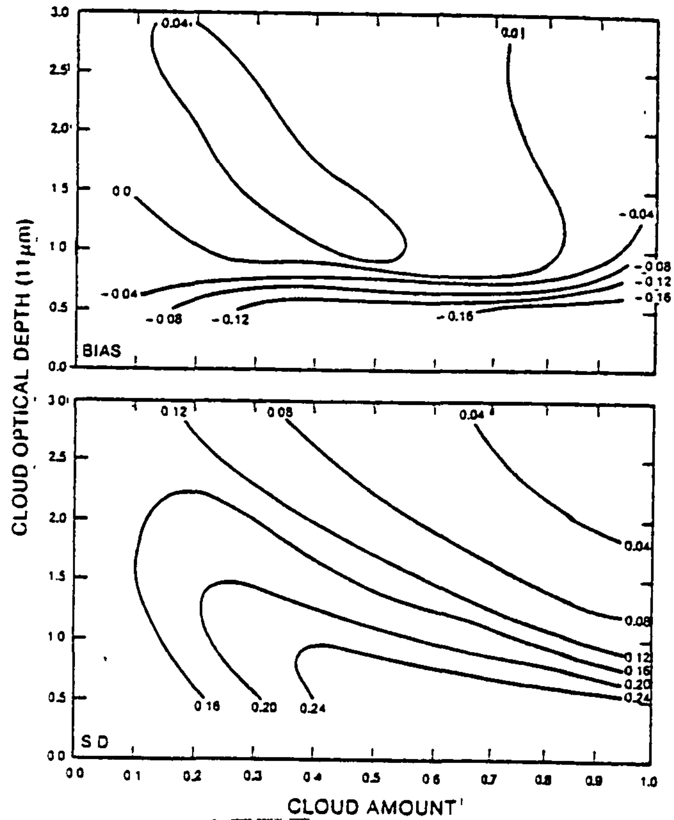

Fig 7c Bias and Standard Deviation of Computed Cloud Amount for Various Assumed Cloud Amounts and Optical Depths (cloud heights assumed at 300 mb).

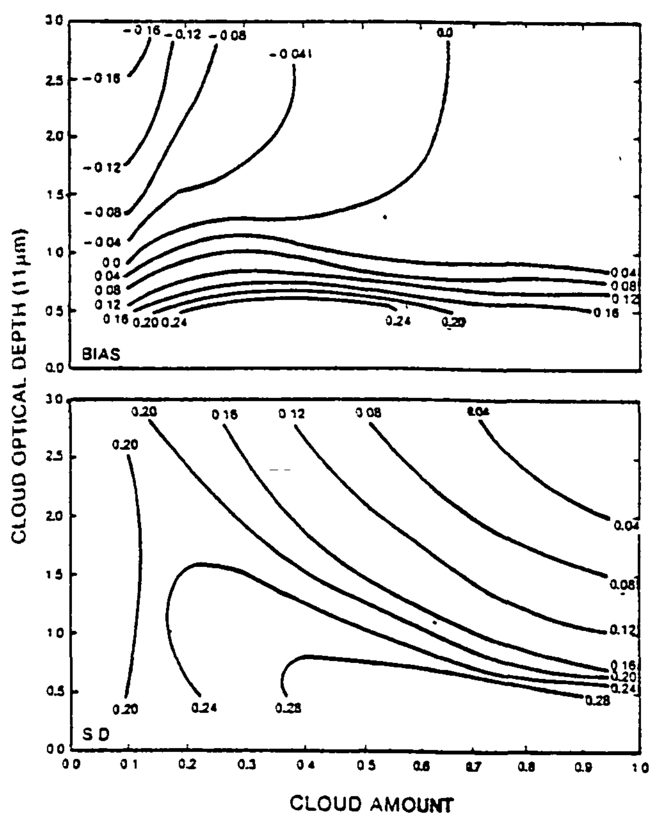

Fig. 7d Bias and Standard Deviation of Computed Cloud Emissivity for Various Assumed Cloud Amounts and Optical Depths (cloud heights assumed at 300 mb)

This is result of the constraint we impose to limit the solution of A to be between 0 and 1. Overall, the results are impressive, because the largest bias of the mean calculated cloud amounts is no worse than -0.18 and the S.D. is no greater than 0.25 for the cases of $0.5<\tau<3.0$.

In Fig. 7d, the mean values of the calculated cloud emissivities and their S.D. are shown. The samples which are counted in for estimating the mean values and S.D. are those determined as cloudy atmospheres in the algorithm. The trend of the calculated cloud emissivity is, in general, opposite to that of calculated cloud amount. The bias of the calculated cloud emissivity is positive for optically thin clouds, but is negative if $\tau>1$. The underestimation of the cloud emissivity for $\tau>2$ is obvious in the small fractional cloud cover areas. This may be because the gradient of percentage distribution for negative Δpq is not distinct when the cloud amount is small. If we review Fig. 3, we find that when the cloud amount is small, the value of Δpq is indifferent with respect to the variations in opical depths.

Next, we test the algorithm for the different cloud heights. We find that for the cloud height assumed to be at 500 mb (~5.72 km), the probability of mistreating a cloudy atmosphere as clear atmosphere decreases compared to that of cloud height at 300 mb. The probability of the cloud-free percentage for cloud amount equal to 0.1 is 26% when $\tau=0.5$ and less than 1% when $\tau=3.0$ as shown in Fig. 8a. In contrast to the conclusions by Wielicki and Coakley (1981), we find that the solution of cloud height retrieval for the lower cloud (at 500 mb) is not worse than the result of higher cloud (300 mb). The accuracy of the cloud height retrieval is dependent on the degree selected for a polynomial describing

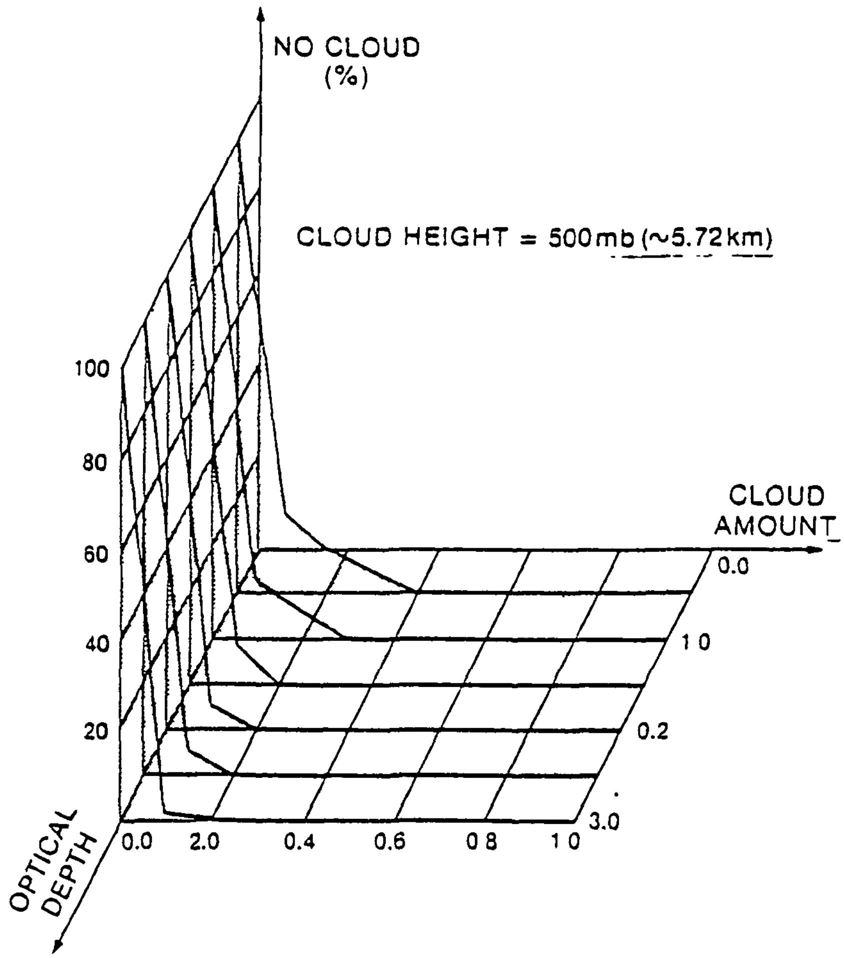

Fig. 8a. Cloud Amount versus Optical Depth (restrictive criterion imposed) for Cloud Ht at 500 mb.

the relation between H function and Z_t in Eq. (9). By using lower degree such as 4 for the polynomial, the cloud height retrieval for the higher cloud may have a better solution than that for the lower cloud. This is because the polynomial of lower degree is better describing the relation of H vs. Z_t for higher cloud. However, the polynomial of higher degree is more suitable for retrieving the lower cloud. The results of the cloud height retrieval based on the polynomial of different degrees for different cloud heights are shown in Table 2. Without imposing measurement noises in the experiment, the inherent bias of the polynomial is shown in the Table. In this study, the polynomial of degree equal to 5 is selected for the calculation.

Table 2. Cloud Height Retrieval Bias: Bias of the cloud height retrieval based on the polynomial of different degrees for different cloud heights.

Z_t (km) \ Degree	4	5	6
9.370	-0.089	-0.173	-0.239
5.720	0.120	-0.069	-0.104
3.078	-0.315	-0.005	-0.008

In Fig. 8.c, the biases of the mean cloud amounts and their S.D. for the cases of cloud height at 500 mb are shown. In general, the patterns of the

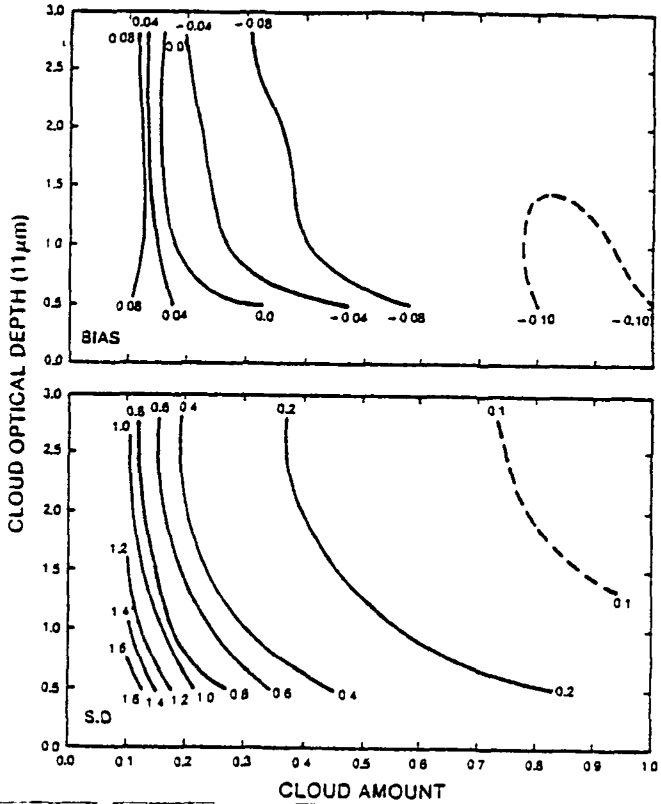

Fig. 8b. Bias and Standard Deviation of Computed Cloud Height for Various Assumed Cloud Amounts and Optical Depths (cloud heights assumed at 500 mb)

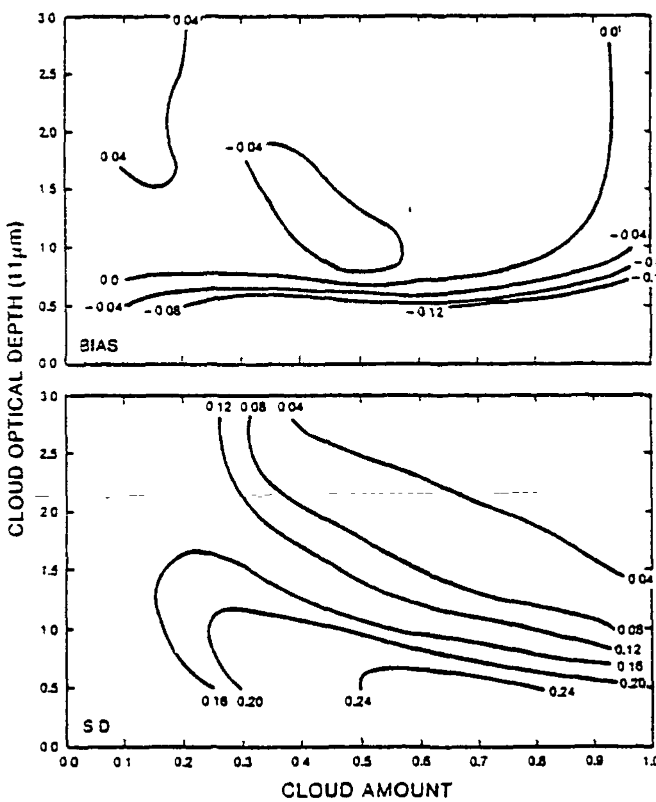

Fig. 8c. Bias and Standard Deviation of Computed Cloud Amount for Various Assumed Cloud Amounts and Optical Depths (cloud heights assumed at 500 mb)

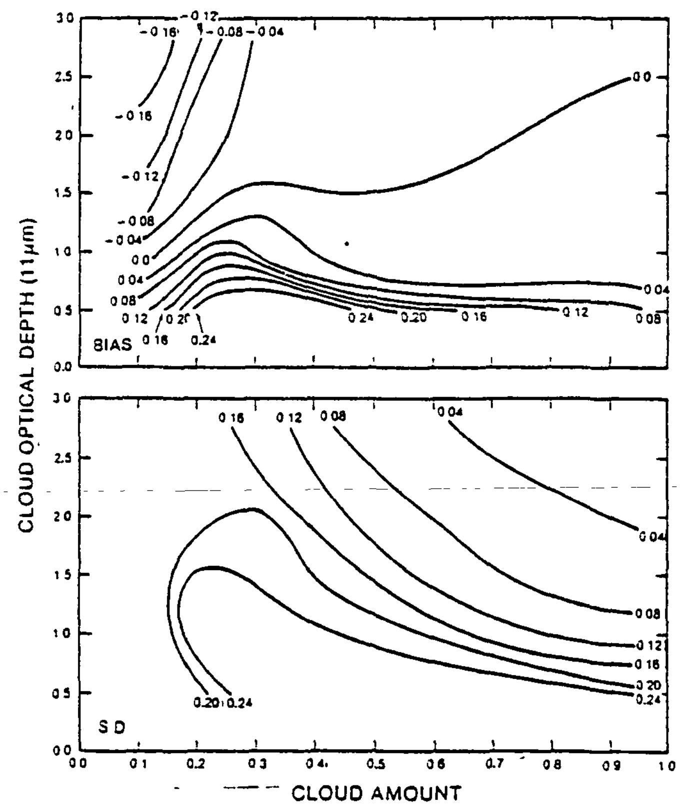

Fig 8d Bias and Standard Deviation of Computed Cloud Emissivity for Various Assumed Cloud Amounts and Optical Depths (cloud heights assumed at 500 mb)

bias and S.D. are quite similar to those at 300 mb height. Since the better solutions of cloud height retrieval result in better estimations of p and q in Eq. (12), and R_m and R_n in Eqs. (20) and (22), respectively, thus the solution of the cloud amount are also improved. The improvements are more evident in the regions of thinner clouds. Finally, the mean value and S.D. of calculated cloud emissivity of cloud height at 500 mb have the same trend as those of cloud height at 300 mb, also with slight improvement of the solutions in thinner clouds region.

For the cloud height at 700 mb (~3.08 km), the results of cloud-free percentage, cloud height, amount and emissivity are shown in Figs. 9a, b, c and d, respectively. The general patterns of the solutions are quite similar to those of cloud heights at 300 and 500 mb. Overall, the solutions for lower clouds are as satisfactory as those for higher clouds.

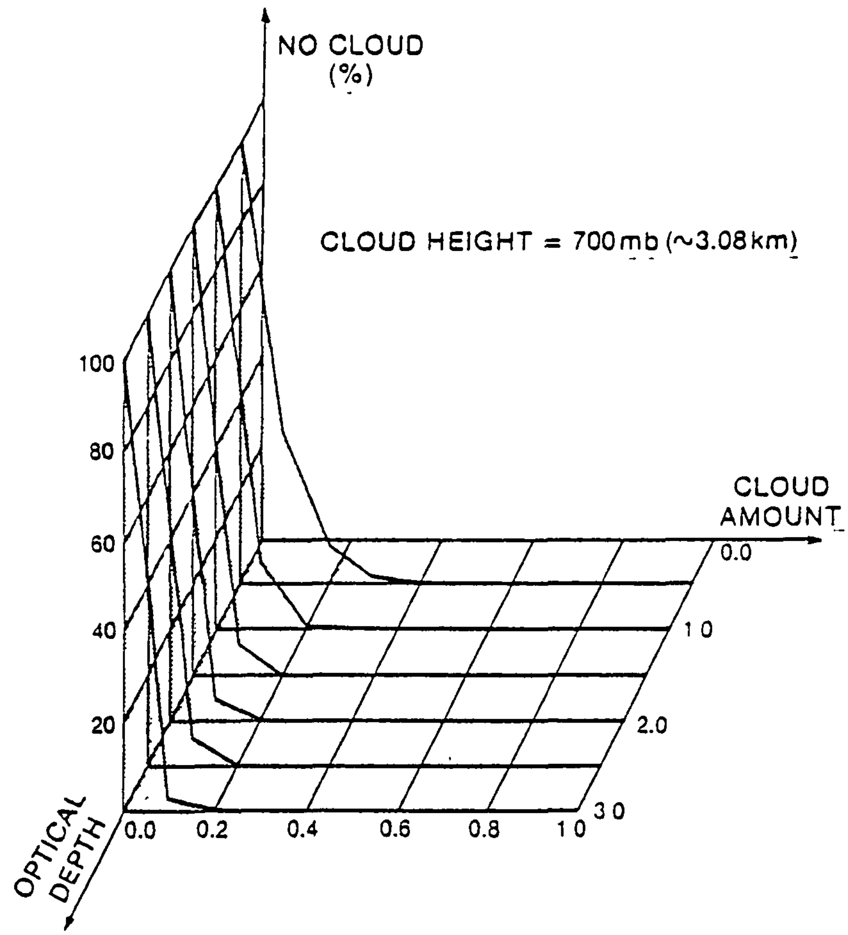

Fig. 9a Cloud Amount versus Optical Depth (restrictive criteria imposed) for Cloud Ht at 700 mb

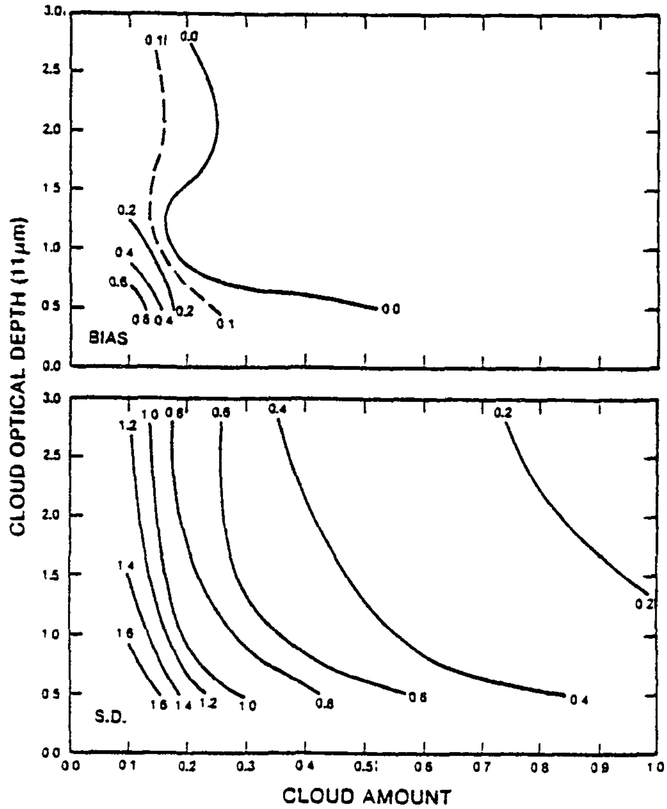

Fig. 9b. Bias and Standard Deviation of Computed Cloud Height for Various Assumed Cloud Amounts and Optical Depths (cloud heights assumed at 700 mb)

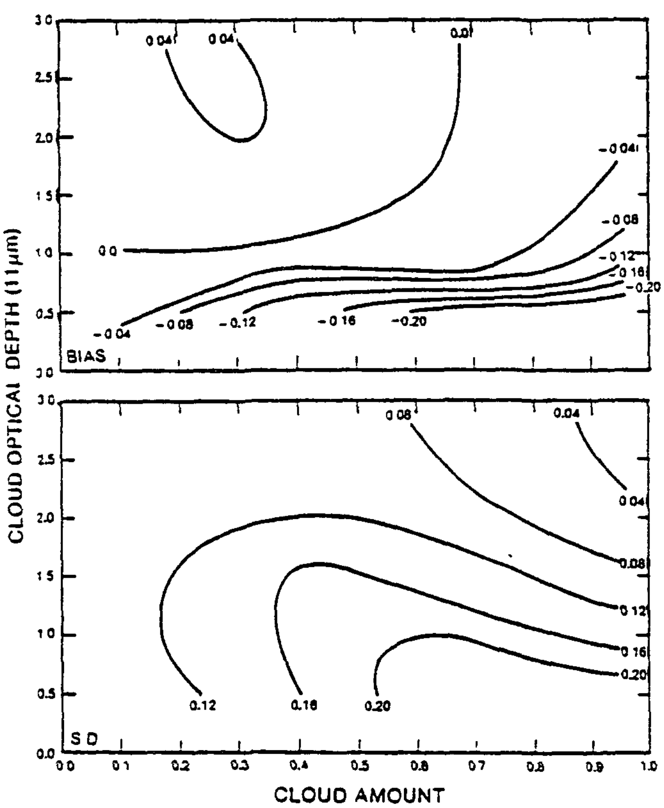

Fig. 9c. Bias and Standard Deviation of Computed Cloud Amounts for Various Assumed Cloud Amounts and Optical Depths (cloud heights assumed at 700 mb)

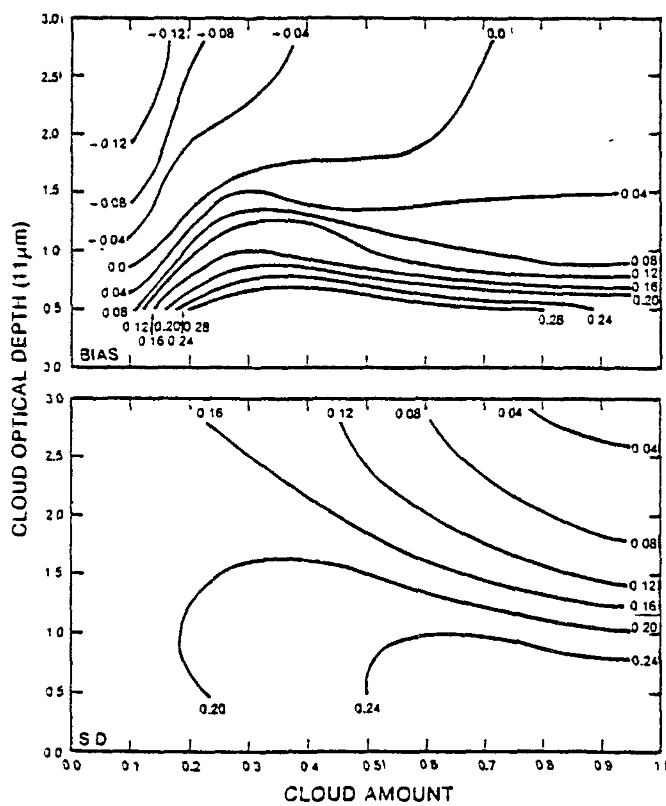

Fig. 9d Bias and Standard Deviation of Computed Cloud Emissivity for Various Assumed Cloud Amounts and Optical Depths (cloud heights assumed at 700 mb)

4. Applications to HIRS/2 data of NOAA 6 and TIROS-N Satellites

On the basis of the previous depiction and analysis it is evident that a proper combination of IR sounder data may be successfully used to recover the cloud parameters. It appears desirable and important to apply the developed retrieval scheme to real satellite data to investigate its applicability. Total number of 28 cases with different synoptic situations were chosen to perform the retrieval exercises. Results are illustrated and will be discussed in this section.

Since NOAA 6 and TIROS-N pass the Great Plains at 1400 and 1000, respectively, the mean value of colocated radiances measured by both satellites may closely represent the observed data at 1200, at which time the RAOB data are available. The RAOB profiles are employed as input data for the calculation of clear atmospheric radiances, and the surface reports are used for the comparsion with the computed results.

There were cases when the RAOB stations did not coincide exactly with HIRS footprints. Because of the horizontal variability of the HIRS data, a distance-weighted method has been devised to obtain an average measured radiance from the available HIRS data around the RAOB station. This procedure is especially important for wing channels which are affected significantly by the surface condition. All of the radiosonde observations used in this study were available up to at least 100 mb.

In this paper, we will present cases on 24 April 1980 along with the GOES-East satellite IR picture (Fig. 10) and the corresponding synoptic observations (Fig. 11). No GOES visible picture will be used, because the

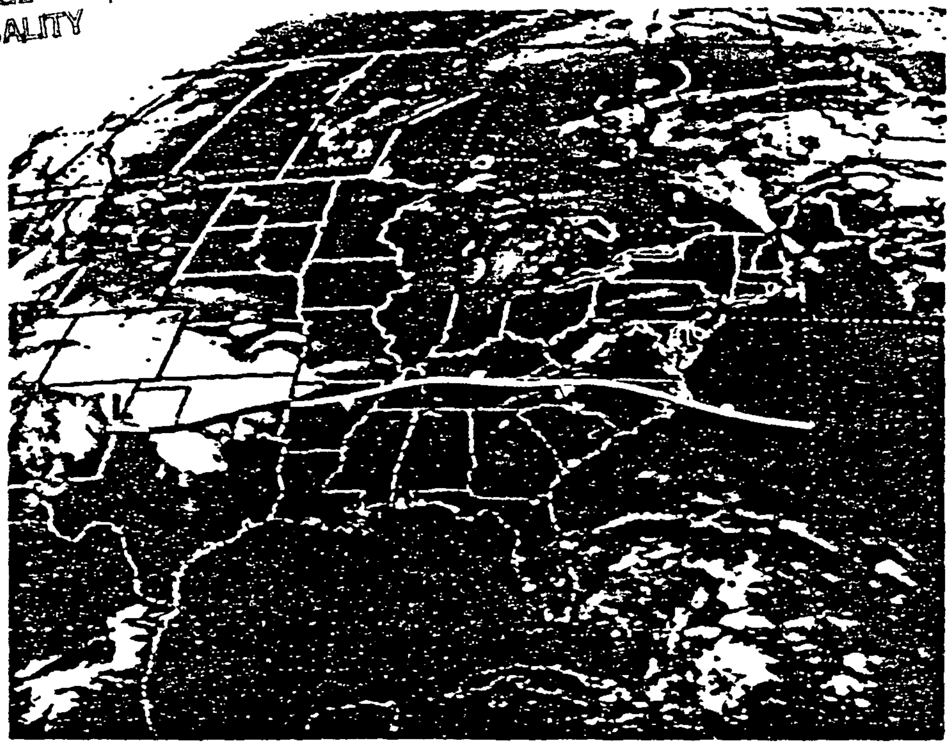

Fig. 10 GOES IR Imagery for April 24, 1980. Imagery is for 1200 GMT with the frontal position shown.

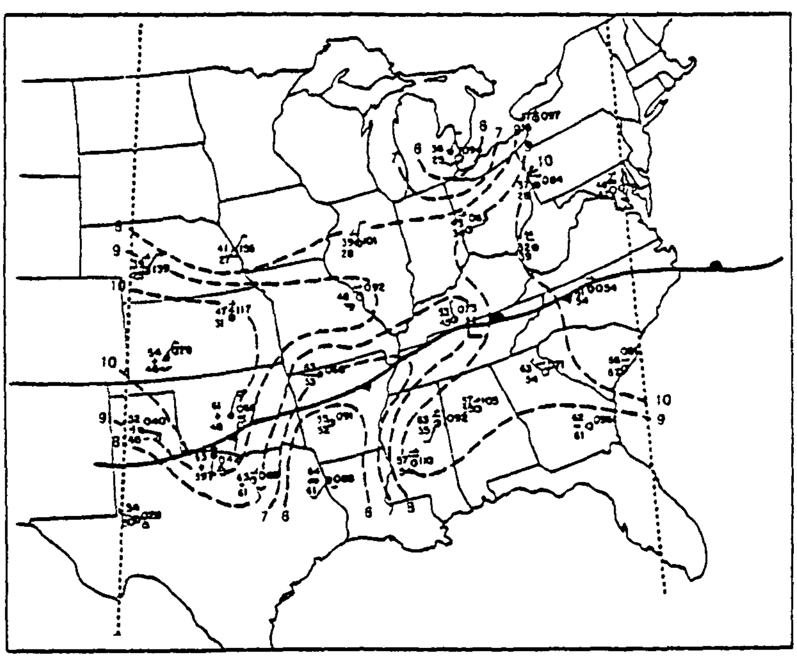

Fig. 11. Computed Cloud Height Analysis. Analysis from HIRS/2 data is shown along with synoptic reports for 1200 GMT 24 April 1980

Great Plains at 1200 was still in dark. On 24 April, there was a low pressure in the eastern Great Plains. The cold front stretched out from the low center to northern Texas, and stationary front extended into the Atlantic Ocean. Analyses of surface reports and GOES image indicate that cirrus clouds were present in the stationary front area, while multi-layer clouds and/or precipitation occurred in the vicinity of the cold front area. Based on the availabity of RAOB profiles, 28 stations were selected for the retrieval exercises. The surface reports of the chosen stations are recorded as shown in Fig. 11, and the results derived from the numerical computations are also plotted.

Results of the cloud height, amount and emissivity retrieval indicate that a strong convective cloud system may exist in large portion of Oklahoma and Kansas states. The high cloud top height, which were found to be as high as 10 km (Fig. 11), and the high emissivity in this area (Fig. 13) suggests that the system is either composed of thick clouds or multi-layer clouds. The cloud amount in this region was close to overcast as shown in Fig. 12.

This convective cloud band is obviously illustrated in the GOES IR picture (Fig. 10), in which the positions of frontal systems are marked. While in the southeast of this cloudy area (eastern Texas and western Lousiana), extensive low clouds were found according to our retrievals. Although these low clouds were not clearly seen from the IR picture, the surface reports confirmed the existence of the clouds. The large values of the cloud amount and emissivity, and the low cloud top height indicate that this might be a less convective area compared to the post-frontal area. The low clouds might have reached the ground, and looked more like fog from some of the surface reports. To the north of the stationary front, extensive cirrus clouds were found. The cloud top heights were at least

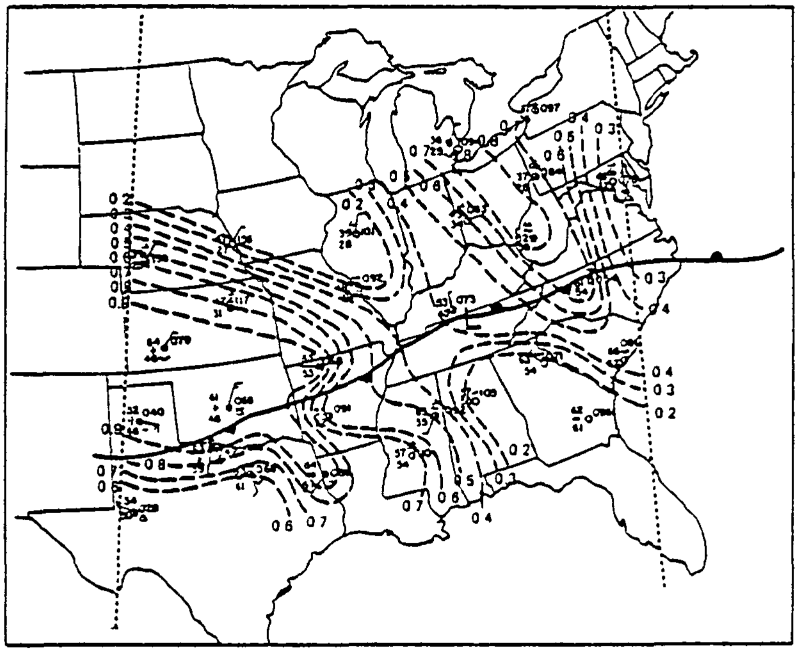

Fig. 12. Computed Cloud Amount Analysis. Analysis from HIRS/2 data is shown along with synoptic reports for 1200 GMT 24 April 1980.

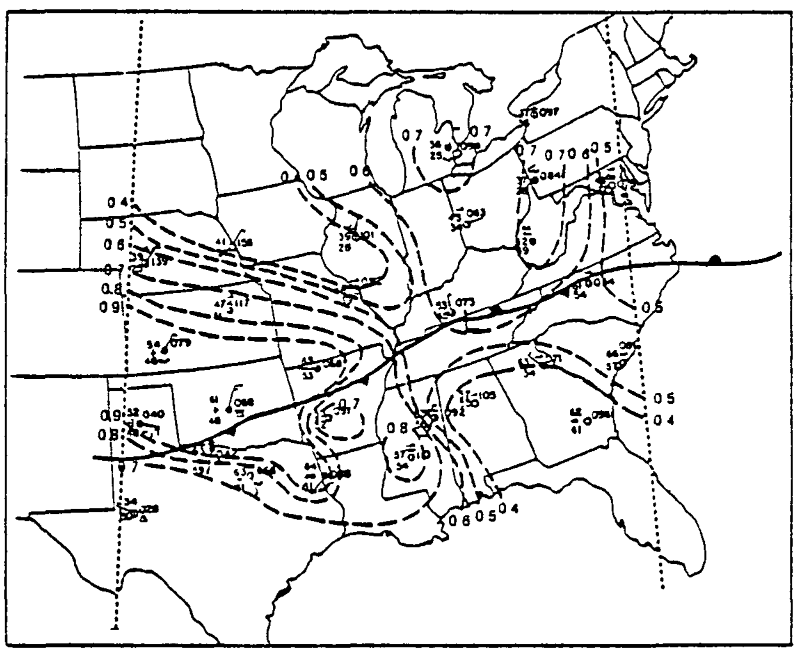

Fig. 13. Computed Cloud Emissivity Analysis. Analysis from HIRS/2 data is shown along with synoptic reports for 1200 GMT 24 April 1980

9 km, and the emissivities were about 0.6. The cirrus clouds in West Virginia might have some scattered low clouds underneath because large values of cloud emissivity (>0.7) were found. There were also large areas of low clouds existing in the southeast of the Great Lakes covering Michigan and northern parts of Illinois and Indiana. To the south of the stationary front, there was largely clear atmosphere with only small fraction of high clouds detected. Those high clouds could be thin cirrus because of small emissivities as the calculated results show.

5. Conclusion

In this study, a numerical method for computing cloud top height, amount and emissivity has been developed based on the parameterized infrared radiative transfer equation for cloudy atmospheres. Theoretical studies were carried out based on synthetic atmosphere containing various thickness of fractional cloud cover within a IFOV. Upon imposing instrument noises to the upwelling radiances the solutions of the cloud parameters under different cloud conditions are obtained. It is found that the measurement error effect is more profound for the thinner and/or smaller fractional cloud case in the numerical calculation. But, in general, resulting cloud parameters retrieved from the present program are found to reasonably accurate by comparision with theoretically assumed solutions. Numerical experiments were also performed utilizing NOAA 6 and TIROS-N HIRS/2 data in which a mesoscale cloud system is analyzed. Numerical results show that the cloud areas were described distinctively in terms of the cloud top height, amount and emissivity derived from the program.

Moreover, the computed cloud height and amount are generally in good comparison with those obtained from synoptic reports and satellite picture. However, further verification of the satellite cloud sounding techniques requires carefully designed field experiments in which reliable cloud properties, such as cloud top height, phase, thickness and emissivity, may be obtained from aircraft observations under the satellite pass.

In application of the current technique to achive cloud information in large scale study (e.g., ISCCP), the satellite radiances have to be arranged in the matrix manner. The entire area within the scale needs to be divided into smaller grid boxes (such as $2.5x2.5^{o}$), in which the radiance histogram can be constructed. The clear column radiance within the grid box can be derived based on the histogram. This clear column radiance may then be used in this cloud retrieval program to replace the clear column radiance computed based on the radiosonde profiles in this study. Such arrangement may significantly save computing time on analyzing large amounts of satellite data. Further study concerning more efficient cloud retrieval technique in the large scale is under investigation and will be reported in future.

6. Acknowledgements

This research was supported by the NRC Resident Research Associateship Program at the Goddard Laboratory for Atmospheric Sciences. The author would like to thank Dr. J. Simpson for the helpful comments. Appreciation is also expressed to Mr. L. Dubach and Ms. K. Wilson for assistance in editing and typing.

7. References

Cess, R. D., 1974: Radiative transfer due to atmospheric water vapor: Global consideration of the earth's energy balance. J. Quant. Spectros. Radiat. Trans., 14, 861-871.

Chahine, M. T., 1982: Remote sensing of cloud parameters. J. Atmos. Sci., 39, 159-170.

Feddes, R. G., and K. N. Liou, 1978: Atmospheric ice and water content derived from parameterization of Nimbus 6 High Resolution Infrared Sounder data. J. Appl. Meteor., 17, 536-551.

Mcclees, D. J., and L. S. Wilson, 1976: Cloud top height from temperature sounding instruments. Quart. J. Roy. Meteor. Soc., 102, 781-790.

Schiffer, R. A., and W. B. Rossow, 1983: The International Satellite Cloud Climatology Project (ISCCP): The first project of the World Climate Research Programme. Bull. Amer. Meteor. Soc., 64, 779-784.

Schneider, S. H., 1972: Cloudiness as a global climatic feedback mechanism: The effects on the radiation balance and surface temperature of variations in cloudiness. J. Atmos. Sci., 29, 1413-1422.

Schwalb, A., 1978: The TIROS-N/NOAA A-G Satellite Series. NOAA Tech. Memo., NESS 95, 75 pp.

Smith, W. L., and C. M. R. Platt, 1978: Comparison of satellite-deduced cloud heights with indication from radiosonde and ground-based laser measurements. J. Appl. Meteor., 17, 1796-1802.

__________, V. E. Suomi, W. P. Menzel, H. M. Woolf, L. A. Sromovsky, H. E. Revercomb, C. M. Hayden, D. N. Erickson and F. R. Mosher, 1981: First sounding results from VAS-D. Bull. Amer. Meteor. Soc., 62, 232-236.

Stephens, G. L., and P. J. Webster, 1979: Sensitivity of radiative forcing to variable cloud and moisture. J. Atmos. Sci., 36, 1450-1466.

Wielicki, B. A., and J. A. Coakley, 1981: Cloud retrieval using infrared sounder data: Error analysis. J. Appl. Meteor., 20, 157-169.

Yeh, H. Y., and K. N. Liou, 1983: Remote sounding of cloud parameterfrom a combination of infrared and microwave channels. J. Clim. Appl. Meteor., 22, 201-213.

__________, T. H. Vonder Haar and K. N. Liou, 1983: Temperature profile and cloud parameters inversion in cirrus cloudy atmospheres. J. Atmos. Sci., (submitted).

BIBLIOGRAPHIC DATA SHEET

1. Report No. TM 86059	2. Government Accession No.	3. Recipient's Catalog No.
4. Title and Subtitle On the Remote Sensing of Cloud Properties from Satellite Infrared Sounder Data		5. Report Date February 1984
		6. Performing Organization Code 914
7. Author(s) H.-Y. M. Yeh		8. Performing Organization Report No.
9. Performing Organization Name and Address NASA/GSFC (Code 914) Greenbelt, MD 20771		10. Work Unit No.
		11. Contract or Grant No.
		13. Type of Report and Period Covered
12. Sponsoring Agency Name and Address NASA/Goddard Space Flight Center (Code 914) Greenbelt, MD 20771		
		14. Sponsoring Agency Code
15. Supplementary Notes		

16. Abstract: A method for remote sensing of cloud parameters by using infrared sounder data has been developed on the basis of the parameterized infrared transfer equation applicable to cloudy atmospheres. The method is utilized for the retrieval of the cloud height, amount, and emissivity in 11 μm region. Numerical analyses and retrieval experiments have been carried out by utilizing the synthetic sounder data for the theoretical study. The sensitivity of the numerical procedures to the measurement and instrument errors are also examined. The retrieved results are physically discussed and numerically compared with the model atmospheres. Comparisons reveal that the recovered cloud parameters agree reasonably well with the pre-assumed values. However, for cases when relatively thin clouds and/or small cloud fractional cover within a field of view are present, the recovered cloud parameters show considerable fluctuations.

Experiments on the proposed algorithm are carried out utilizing High Resolution Infrared Sounder (HIRS/2) data of NOAA 6 and TIROS-N. Results of experiments show reasonably good comparisons with the surface reports and GOES satellite images.

17. Key Words (Selected by Author(s)) Cloud Observations; Satellite IR cloud sensing; TIROS-N HIRS/2; NOAA 6	18. Distribution Statement No restriction

19. Security Classif. (of this report) Unclassified	20. Security Classif. (of this page) Unclassified	21. No. of Pages 47	22. Price*

*For sale by the National Technical Information Service, Springfield, Virginia 22151. GSFC 25-44 (10/77)